OXFORD

Original Article

Automated quantification of vomeronasal glomeruli number, size, and color composition after immunofluorescent staining

Shahab Bahreini Jangjoo[1],*, Jennifer M. Lin[2,3],*, Farhood Etaati[4], Sydney Fearnley[5,6], Jean-François Cloutier[5,6,7], Alexander Khmaladze[1] and Paolo E. Forni[2,3]

[1]Department of Physics, University at Albany, Albany, NY, USA, [2]Department of Biological Sciences, University at Albany, Albany, NY, USA, [3]The RNA Institute, University at Albany, Albany, NY, USA, [4]School of Electrical and Computer Engineering, College of Engineering, University of Tehran, Tehran, Iran, [5]The Neuro, 3801 University, Montréal, QC H3A 2B4, Canada, [6]Department of Anatomy and Cell Biology, McGill University, Montréal, QC, Canada and [7]Department of Neurology and Neurosurgery, McGill University, Montréal, QC, Canada

Corresponding author: Paolo E. Forni, Department of Biological Sciences, The RNA Institute, University at Albany, Albany, NY, USA. email: pforni@albany.edu

*These authors contributed equally to this study.

Editorial Decision 23 August 2021.

ABSTRACT

Glomeruli are neuropil-rich regions of the main or accessory olfactory bulbs (AOB) where the axons of olfactory or vomeronasal neurons and dendrites of mitral/tufted cells form synaptic connections. In the main olfactory system, olfactory sensory neurons (OSNs) expressing the same receptor innervate 1 or 2 glomeruli. However, in the accessory olfactory system, vomeronasal sensory neurons (VSNs) expressing the same receptor can innervate up to 30 different glomeruli in the AOB. Genetic mutation disrupting genes with a role in defining the identity/diversity of olfactory and vomeronasal neurons can alter the number and size of glomeruli. Interestingly, 2 cell surface molecules, Kirrel2 and Kirrel3, have been indicated as playing a critical role in the organization of axons into glomeruli in the AOB. Being able to quantify differences in glomeruli features, such as number, size, or immunoreactivity for specific markers, is an important experimental approach to validate the role of specific genes in controlling neuronal connectivity and circuit formation in either control or mutant animals. Since the manual recognition and quantification of glomeruli on digital images is a challenging and time-consuming task, we generated a program in Python able to identify glomeruli in digital images and quantify their properties, such as size, number, and pixel intensity. Validation of our program indicates that our script is a fast and suitable tool for high-throughput quantification of glomerular features of mouse lines with different genetic makeup.

Key words: glomeruli, automated quantifications, adaptive threshold, vomeronasal organ, accessory olfactory bulb

Introduction

An important aspect in neuroscience is the identification of genes responsible for synaptic target specificity. Guidance cues, surface molecules, and cell adhesion molecules are key players in axon guidance and synapse formation across different types of neurons (Cloutier et al. 2002; Dean et al. 2003; Martin et al. 2015). Vomeronasal sensory neurons (VSNs) located in the vomeronasal organ express

vomeronasal receptors (VRs), which detect certain chemosignals and transduce those signals to the accessory olfactory bulb (AOB) in the brain.

Most of the neurons of the vomeronasal epithelium (VNE) belong to 2 main populations, which detect different types of pheromones and play different roles in elicited social responses. VSNs located in the apical region of the VNE express members of the VR type 1 (V1rs) family, which transduce their signal through the Gαi2 G-protein subunit, express the transcription factor (TF) Meis2 and the guidance cue receptor Nrp2 (Dulac and Axel 1995; Enomoto et al. 2011). These neurons project their axons to the anterior portion of the AOB. VSNs located in the basal region of the VNE express vomeronasal type 2 receptors (V2rs) (Silvotti et al. 2011), transduce their signal through the Gαo G-protein subunit, express the TF AP-2ε (Enomoto et al. 2011; Lin et al. 2018), and the guide cue receptor Robo2. These neurons project their axons to the posterior AOB (Fig. 1). A third subtype of VSNs express Formyl peptide receptors (Fprs) (Bufe et al. 2012; Liberles et al. 2009; Riviere et al. 2009). Neurons expressing mFpr-rs1 also express Gαo, whereas Gαi2 expressing neurons can express mFpr-rs3, mFpr-rs4, mFpr-rs6, and mFpr-rs7 (Riviere et al. 2009; Bufe et al. 2012). Proper differentiation, organization, and signaling in VSNs are necessary for their individual roles in integrating external cues and translating them into behaviors (Del Punta et al. 2002; Stowers et al. 2002; Chamero et al. 2011, 2017; Brignall and Cloutier 2015).

Glomeruli are neuropil-rich regions of the olfactory bulbs where the axons of olfactory or vomeronasal neurons and dendrites of mitral/tufted cells form synaptic connections. The organization of axons and the glomeruli they innervate largely relies on the type of olfactory/VR gene expressed by individual neurons. The main olfactory sensory neurons (OSNs) expressing the same receptor innervate 1 or 2 glomeruli. However, in the accessory olfactory system,

VSNs expressing the same receptor can innervate up to 30 different glomeruli in the AOB (Belluscio et al. 1999; Rodriguez et al. 1999).

The fasciculation of the vomeronasal axons and formation of synaptic connections with their targets in the brain are mediated by the guidance molecules, by the VR(s) expressed, and by complex expression of cell surface molecules (Brignall and Cloutier 2015). The Kirrel family of cell surface molecules has been previously shown to play a relevant role in controlling axon coalescence in the olfactory and vomeronasal systems (Serizawa et al. 2006; Prince et al. 2013; Vaddadi et al. 2019). Combinatorial expression of Kirrel2 and Kirrel3 in VSNs assists in the formation and organization of glomeruli in the AOB. Notably, neurons projecting to the anterior portion of the AOB mostly express Kirrel2, whereas the basal neurons, projecting to the posterior AOB, are mostly positive for Kirrel3 (Fig. 3B) (Prince et al. 2013; Brignall and Cloutier 2015).

When experimentally analyzed, glomeruli are usually hand traced on digital images to generate regions of interest (ROIs), which can then be analyzed for the number, size, and color composition or intensity using image analysis software, such as ImageJ (Prince et al. 2013; Naik et al. 2020). On histological sections glomeruli are commonly identified as OMP-positive and/or VGluT2-positive structures surrounded by a noninnervated region (Prince et al. 2013).

Notably, human made identification of glomeruli can be inconsistent, as it is dependent on the investigators′ ability to recognize complex morphological structures. These factors can compromise consistency in measurement when images are analyzed by different researchers. Additionally, this kind of analysis is usually tedious and time consuming. Due to the lack of defined borders and heterogeneity of the shapes and sizes of glomeruli in the AOB, existing methods of automated analysis are either not suitable for quantification of glomeruli or require specialized techniques, such as 3-dimensional imaging of solvent-cleared organs, and costly software, to identify and quantify these structures (Zapiec and Mombaerts 2015; Rizzardi et al. 2016). In order to facilitate this process and increase consistency, we generated an image processing program in Python that can be used to quantify glomeruli size, number, and immunostaining intensity. The program employs OpenCV, which is an open source image processing library (Bradski 2000) that has been previously used in biological applications to identify patterns in a digital image (Uchida 2013; Cosentino et al. 2015; Dominguez et al. 2017; Obando et al. 2018; Lutnick et al. 2019). Our software separates multichannel images into single color images, uses adaptive thresholding to identify patterns, and quantifies features, such as area, number of objects, and intensity for the selected channels.

We validated our bioinformatic tool and tested various parameters on samples of previously published wild-type (WT) controls and mutant animals carrying genetic mutations affecting glomeruli protein expression, size, and number (Prince et al. 2013). By comparing human and automated identification of glomeruli, we noticed obvious differences in what would be considered one or multiple glomeruli. However, when normalized, the discrepancies between manual and automated quantifications did not compromise the detection of significant differences between genotypes. Our data suggest that our script can be used as a suitable tool to perform high-throughput analysis of glomeruli features and identify differences between mice with different genetic makeup.
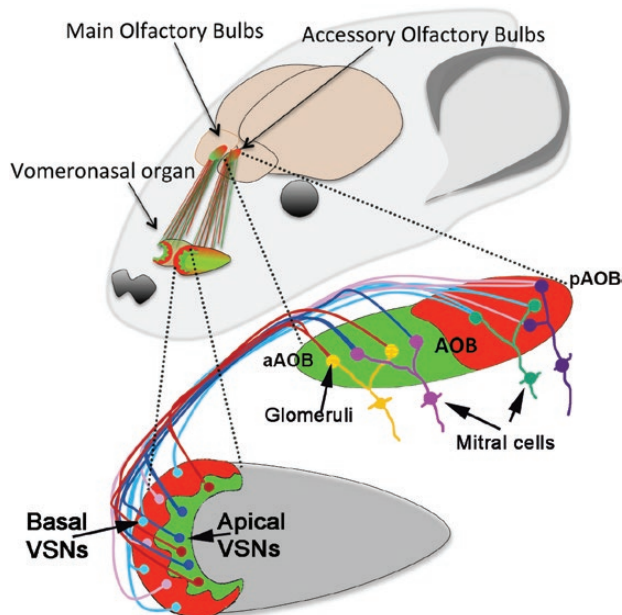
Fig. 1. Cartoon of mouse head. The VNO projects to the accessory olfactory bulb (AOB) (red, green). Schematic of the vomeronasal epithelium: VSNs in the apical region (green) project to the anterior AOB (aAOB, green), whereas VSNs in the basal areas (red) project to the posterior AOB (pAOB, red). VSNs, based on the receptor that they express (indicated by different colors: cyan, pink, blue, and red), connect with specific mitral cells in the AOB (yellow, magenta, green, and purple) forming distinct glomeruli in the AOB.

Materials and methods

Animals

Adult WT or Kirrel3 KO mice (Prince et al. 2013) were used for all analyses. All data were collected from mice kept under similar

housing conditions, in transparent cages on a normal 12 h light/dark cycle. Tissue collected from males and females in the same genotype/treatment group were combined; ages analyzed are indicated in text and figures.

Immunohistochemistry

Adult mice were anesthetized and then transcardially perfused with 4% paraformaldehyde in phosphate-buffered saline (PBS). Brain tissue was isolated at the time of perfusion and cryofixed in PBS containing 30% sucrose as previously described in Prince et al. (2009).

Citrate buffer (pH 6.0) antigen was performed for all the antibodies indicated with asterisks (*). Primary antibodies and concentrations used in this study were Goat anti-Nrp2 (1:4000, AF567, R&D Systems, Minneapolis, MN), Goat anti-OMP (1:4000, 5441001, WAKO, Osaka, Japan), *Mouse anti-Robo2 (1:250, sc-376177, Santa Cruz, Dallas, TX). *Bandeiraea simplicifolia* (BS)-Lectin (1:1500; Vector Laboratories, Burlingame, USA) was applied with the secondary antibody.

Manual quantification of glomeruli structure and formation

Selection of glomeruli was performed on 20-μm parasagittal cryosections of adult mice immunostained with markers expressed by the glomeruli in the AOB and imaged through confocal microscopy. Glomeruli in the anterior and posterior regions of the AOB were defined as discrete regions of OMP+ or VGluT2+ axonal endings with similar composition of Kirrel2 and Kirrel3 expression that differ from neighboring regions. Anterior and posterior regions of the AOB were identified based on differential staining against Nrp2, Robo2, and BS-Lectin. Manual quantifications for glomerular size, number per section, and immunoreactivity were performed on confocal images using FIJI 2.1.0.

Image preparation for automated analysis

Confocal images were imported into FIJI 2.1.0, where the relevant Z-stacks were combined using Maximum Intensity Z-projection. In this article, we utilized a range of 4–6 focal planes for the Z-stack. The individual ROIs were generated by identifying the anterior and posterior glomerular regions of the AOB through morphological and histological means. The area outside of the desired region was cropped out to limit quantification of extraneous regions. All images were saved as TIFF files to preserve the individual channels.

Development of image analysis program

This program was written in Python 3 generation programing language. The images were subjected to thresholding, which was done by ADAPTIVE_THRESH_GAUSSIAN_C method in OpenCV, to convert images into binary. Also, the constant subtraction value for chosen Gaussian thresholding was set to 4 for all images. This specific method required a set block size, which determined the number of pixels surrounding a given pixel that should be considered to set the threshold limit. The threshold for each pixel was then set by comparing the pixel intensity to the average intensity of all the pixels in the block. The object identification was performed using 3 different square block sizes to check the program output sensitivity for this parameter. Smaller block sizes consider smaller area in the pixel proximity and result in smaller identified objects on average.

For glomeruli identification, the program used OpenCV library and its "contours" tool. RETR_EXTERNAL flag (also known as "parent contours") was implemented to pick the outermost regions of identified objects and ignore all inside complexity, such as holes. Another restriction for the detected patterns was the size limit. This limit set a minimum threshold to ignore all miniscule contours. All processes were tested for 6 different minimum size limits to check how this parameter affects the ability to detect phenotypic differences between control and WT animals. Our open source program was able to analyze over 100 confocal images in less than 90 s with any affordable CPU and GPU PC or laptop (In our case, Intel 4th Gen Core I7 MQ series, Nvidia Quadro K1100 M).

In this article, we only used block size and minimum size limit to identify glomeruli; however, other functions that may assist in glomeruli detection and/or limit the identification of objects that are not glomeruli (e.g., nerve fibers), such as morphology filter tools (i.e., circular filter, ellipse filter, ratio filter), histograms, and selection filters are still in development.

Instructions for installation, program requirements, and access to the code are available as Supplementary Data at https://github.com/ForniLab/Glomeruli-Analyzer.

Experimental design and statistical analysis

Data from the automated analysis were generated for the area (number of pixels) and the average intensity level per pixel. Manual data were generated for the area in μm^2 and the intensity as corrected total fluorescence level per μm^2. Data from the manual and automated analyses were exported to Microsoft Excel. For each experiment, we analyzed at least 3 samples per genotype/condition. The values (size, number of glomeruli, intensity) for each sample were averaged as one datapoint. Averaged data were imported and analyzed using GraphPad Prism9. Comparison of manual and automated values was performed on normalized values to the average of each dataset. Sample sizes and *P*-values are indicated as single points in each graph and/or in figure legends. The data are presented as mean ± SEM. Two-tailed, unpaired *t*-tests were used for all statistical analyses, and calculated *P*-values < 0.05 were considered statistically significant.

Automated analysis of images using Gaussian adaptive thresholding

The human identification of glomeruli is based on prior knowledge or an expectation of a probable shape. Therefore, the experience and personal preferences can affect manual selection of glomeruli (Beck and Kastner 2009).

Our goal when developing this program was to identify "objects"/ROIs based on continuous regions of color composition and intensity.

As a first step, the software separates multichannel (Fig. 2A) images into individual channels (Fig. 2B). The target colors and staining are supposed to represent glomeruli areas as illuminated regions (Fig. 2C). To identify distinct patterns, based on relative intensity, we used adaptive Gaussian threshold (Otsu 1979) (Fig. 2D). This thresholding technique is based on the relative intensity of neighboring regions. The threshold for each pixel is set by comparing the intensity of each pixel to the average intensity of the pixels in the surrounding area. The surrounding area is a square region called "block," and the number of pixels included in this area is referred to in this article as "block size." If the average intensity of all the pixels in the block is greater than the intensity of the pixel, the pixel is discarded.

To identify glomeruli, the binary channels are processed by OpenCV library contour finding function to seek all possible
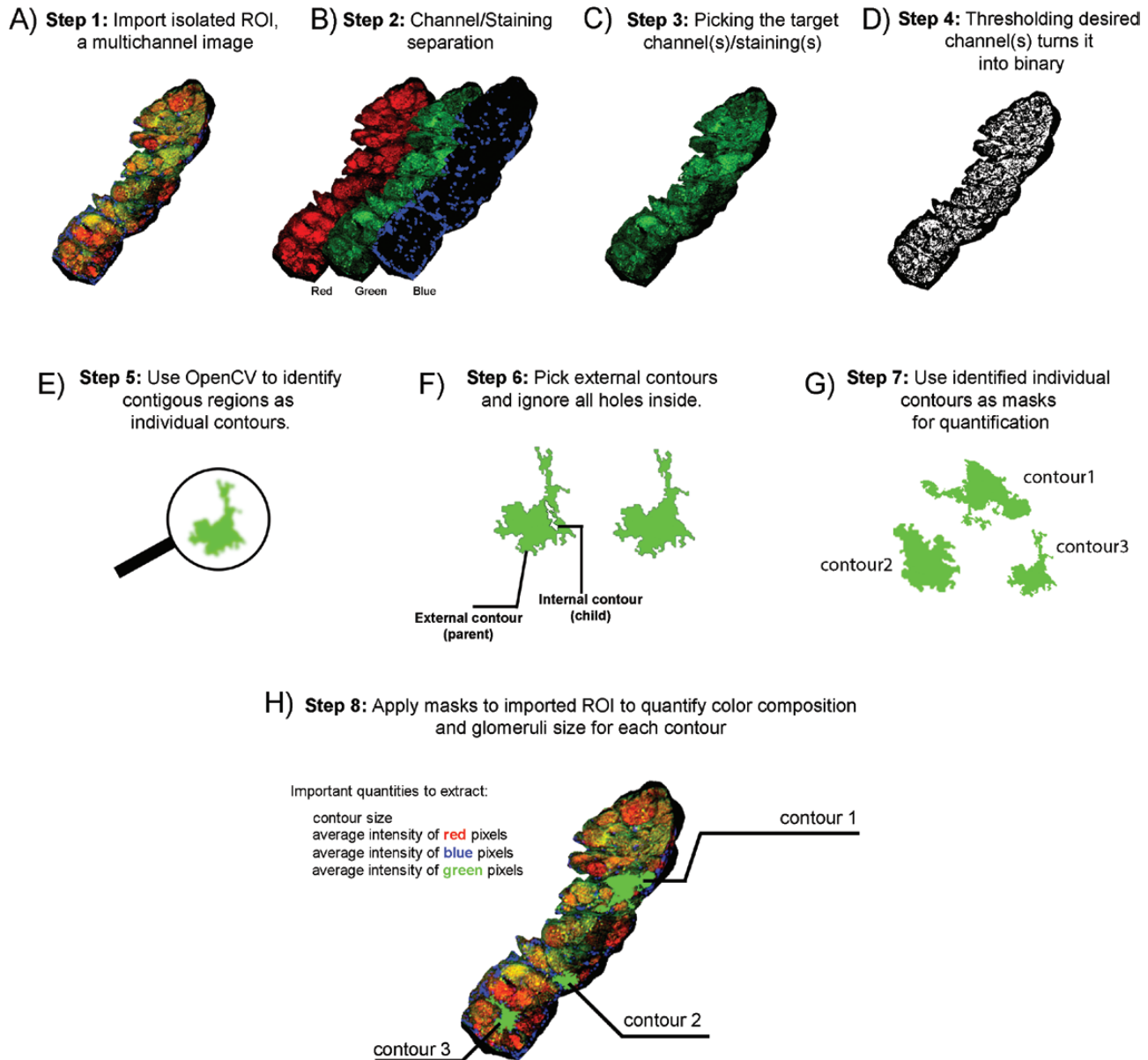
Fig. 2. Diagram showing how the program identifies putative glomeruli in an ROI. A) The multichannel image of the anterior or posterior AOB (a multicolor image) is imported. In this RGB image, the channels are stains against BS-Lectin (red), olfactory marker protein (OMP, green), and Hoescht (blue) counterstain, respectively. B) Split channels to isolate the separate stains. C) Choose the channel with the specific marker expressed by the glomeruli. D) Gaussian adaptive threshold is applied to the selected channel. E) The binary image is fed into the contour OpenCV algorithm to find all available objects and record all identified objects and their locations. F) Use pattern recognition to select only the outermost/external contours (parent contours) and ignore all holes inside the identified objects/contours (child contours). G) Use the previously identified patterns/contours to create masks and crop their location from the originally imported image, and analyze the region. H) Using these masks, the program finds average intensity for each channel (e.g., red, green, and blue) for each of the previously identified contours from the original image. The program exports data for the number of identified contours in the entire image, average color intensities per contour, and average contour size (number of pixels) for the imported image.

external contours (Fig. 2E). The contour size is defined as all pixels that are enclosed by the contour border. Contours can be as small as one pixel in size. To discriminate between objects of interest and noise we set minimum size limits for the identified contours (Fig. 2F). Throughout this article, we set different block sizes and minimum size limits to test the influence of these parameters in identifying distinct glomeruli (see Fig. 4). This program extracts average pixel intensity and the size per contour and records their numbers in aAOB and pAOB by creating masks out of identified contours (Fig. 2G).

Results and discussion

Detection and quantification of glomeruli size and immunoreactivity in the anterior and posterior AOB of wild-type animals

We tested our script on histological sections of the AOB of adult WT mice, where glomeruli of the anterior and posterior AOB were previously manually identified and traced based on immunoreactivity against Robo2, Nrp2 (Fig. 3A), anti-VGluT2 (Fig. 3A′), Kirrel2, Kirrel3 (Fig. 3B), and anti-VGluT2 (Fig. 3B′). The manually made

ROIs for the glomeruli were used to quantify the average glomerular size (µm²), and average number of glomeruli in aAOB and pAOB per section. The same ROIs were used to quantify the average immunoreactivity for Kirrel2 and Kirrel3 for the glomeruli in each region.

For automated quantification, our script was able to identify glomeruli in the aAOB (Fig. 3C) and pAOB (Fig. 3C′). Dashed rectangles show the same regions in the anterior AOB (Fig. 3B′ and C) and posterior AOB (Fig. 3B′ and C′). The magnified selections of the anterior are shown in Fig. 3D and D′, and the magnified selection for the posterior are shown in Fig. 3D″ and D‴. Figure 3D and D″ are resulting glomeruli identified by the program, and Fig. 3D′ and D‴ are the manually identified glomeruli. Here, the blue channel (VGluT2) was used, the adaptive threshold block size was set to 101, and all contours below 40 pixels in size were discarded. The presumptive glomeruli areas identified by the program after thresholding appeared obviously smaller and surrounded by sharper edges compared to what can be identified by humans on non-naive images (Fig. 3D and D‴). The automated selection yielded glomerular area (number of pixels), the number of glomeruli per section, and immunofluorescence intensity. To compare the automated and manual methods, the values for glomerular area (Fig. 3E), the number per section (Fig. 3F), and differential immunoreactivity for Kirrel2 and Kirrel3 (Fig. 3G) in anterior and posterior AOBs were normalized to the average of each dataset. The automated quantification produces results similar to the human made quantification, which confirmed validity of the automated approach.

A comparison of human and automated quantification of Kirrel3 mutants vs. controls

To understand whether this program was capable of detecting the differences in glomerular organization between mice carrying different genetic mutations, we analyzed the image sets used to generate the previously published data for WT controls (Fig. 4A) and Kirrel3 KO (Fig. 4B) mutant mice, where the glomeruli in the pAOB were estimated to be approximately twice as large and about half as many glomeruli in number, when compared with WT controls (Prince et al. 2013). The confocal images were divided into separate sets of images, containing either anterior or posterior AOBs for each animal and condition, before being put through the automated analysis (as illustrated in Fig. 3C and C′).

To evaluate how the block size and minimum size limit would affect the detection of significant differences between the WT and Kirrel3 Kos, we compared the resulting values obtained with different combinations of block size and minimum size limit through statistical analysis. The *P*-values from these analyses were graphed for glomerular size in the aAOB (Fig. 4C) and pAOB (Fig. 4D), as well as average number of glomeruli per section for the aAOB (Fig. 4E) and pAOB (Fig. 4F). We found that setting the block size at 101 pixels selected most of the glomerular layer and allowed us to detect consistent statistical differences between genotypes in the size (Fig. 4C and D) and the number of glomeruli (Fig. 4E and F) in both anterior and posterior regions, when minimum size limits were implemented.

To test the effect of various minimum size limits on detecting putative glomeruli across genotypes (compared with manually selected glomeruli in Fig. 4G–J), we analyzed samples of Kirrel3 KOs and WT controls, implementing different size minimums, and then compared the average size and number of glomeruli for each condition. The results of these observations indicated that without setting a minimum size limit (Limit 1, Fig. 4K and M), we could not detect significant

differences in size (Fig. 4K) and number (Fig. L) of glomeruli between WT controls and Kirrel3 KOs. However, setting a minimum size limit of 60 pixels allowed us to detect and confirm previously published differences between the size (Fig. 4M) and the number of glomeruli per section (Fig. 4N) in the pAOB (Prince et al. 2013). Notably, by setting limit sizes, and therefore creating specific cutoffs in the identification of the ROIs, we also identified small but significant differences in the size (Fig. 4L) in the aAOB, which were not previously detected manually (Prince et al. 2013).

We found by testing these parameters that block size has a great influence on the regions recognized as glomeruli. In fact, by changing the block size, we were able to obtain higher resolution in the identification of glomeruli as individual ROIs. By setting different values for block size (51, 101, 201 pixels) on the same biological samples, we identified the block of 101 pixels as the setting that yielded selections similar to the manually made ROIs. These observations suggest that running comparative analysis with different block sizes could facilitate the identification of differences that can be further validated by human measurements (Fig. 4).

Moreover, we found that limiting the number of small artifacts detected by the program is essential for detecting statistically significant differences between phenotypes (Fig. 4C–F). By analyzing samples from mutant mice that have been shown to have aberrant glomeruli size and number, we observed that setting the minimum size for object recognition is necessary to detect significant differences across samples. In fact, when no minimum size limit was implemented, the previously reported phenotypic differences between Kirrel3 KO mutants and WT controls could not be detected either for the glomeruli size (Fig. 4K) or number (Fig. 4M). However, by experimenting with different settings of the block size and minimum size limits, we found that, for our experimental conditions, using the block size of 101 pixels and a minimum object size limit of 60 pixels, we were able to recapitulate the published differences between size (Fig. 4L) and number of glomeruli (Fig. 4N) in the pAOB between WT and Kirrel3 KOs (Prince et al. 2013). Notably, by using consistent parameters for glomeruli detection and setting minimum limit sizes, thus creating specific cutoffs for the inclusion of identified ROIs, we also found subtle but significant differences in the size of the glomeruli in the aAOB (Fig. 4M) that were not previously detected by manual quantification (Fig. 4C and D). These data, if further confirmed, could point to previously undetected effects of Kirrel3 mutation on neuronal populations.

The glomeruli of the AOB are heterogenous in size and the boundaries of these glomeruli are generally more difficult to define when compared with the MOB (Meisami and Bhatnagar 1998). The automated identification and quantification of heterogeneous regions and structures remains a challenging task that requires specialized equipment and techniques that can be cost prohibitive (Zapiec and Mombaerts 2015; Rizzardi et al. 2016). The free software available for automated image analysis is often focused on identifying cells in culture or tissue or uniform structures and often requires the knowledge of basic coding to function (Lamprecht et al. 2007).

In this article, we present a new and free bioinformatic tool that allows us to perform automated quantification of heterogeneous structures, such as glomeruli in the AOB of rodents, using adaptive thresholding, which considers local differences in pixel intensity of a single marker (OMP or VGluT2) to identify regions that may be missed by using global thresholding, such as low intensity areas. Using this program, we were able to perform rapid systematic comparative analysis of AOB glomeruli size, number, and immunoreactivity between mice with different genetic makeup by
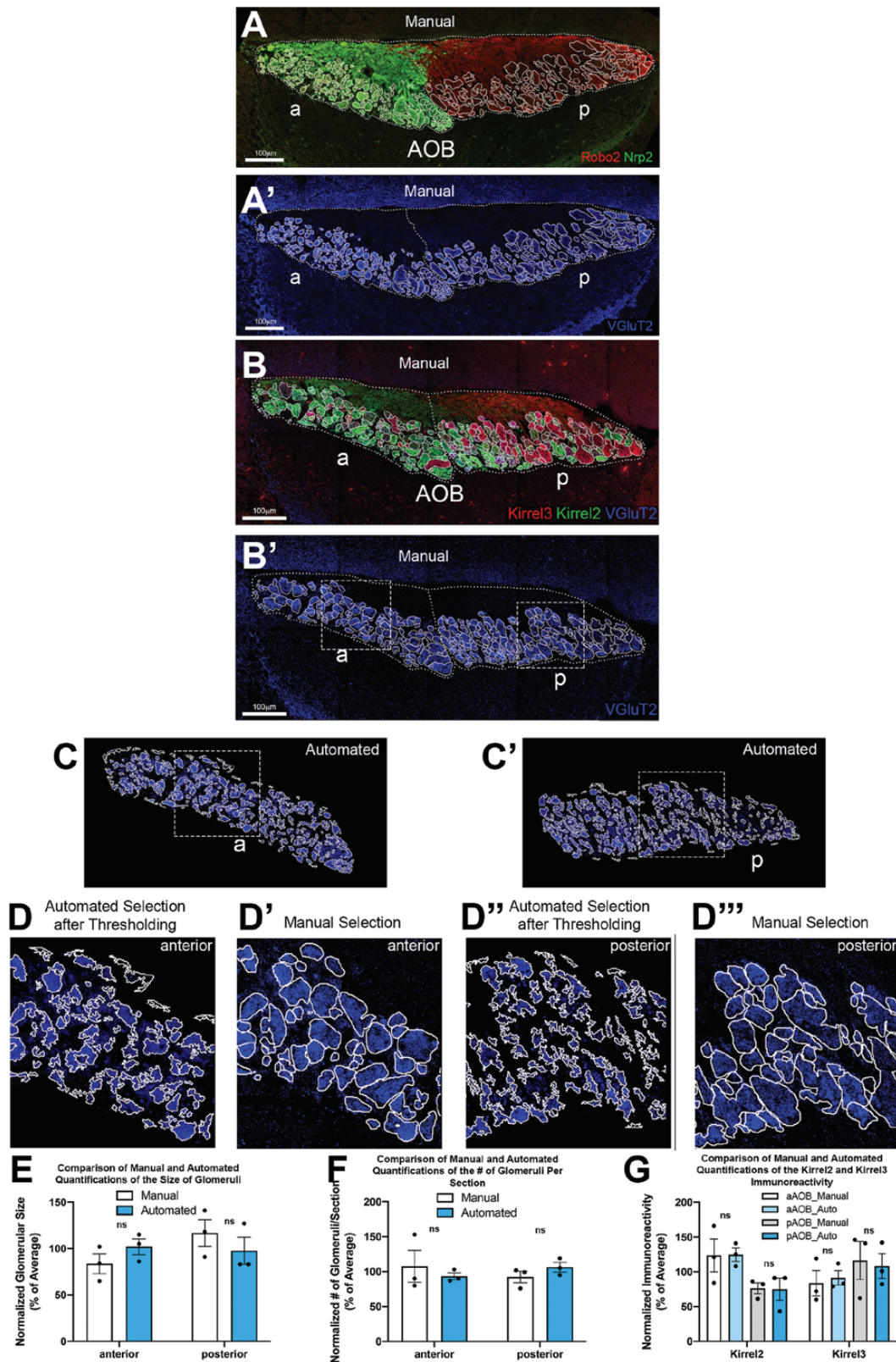
Fig. 3. Comparison of manual and automated selection of glomeruli in the anterior and posterior regions of the accessory olfactory bulb (AOB) in an adult wild-type mouse. The VGluT2 (blue) positive glomeruli (block size 101 pixels and limit size of 40 pixels has been set for this analysis). A′, B′) in the AOB were manually identified and traced throughout the anterior (a) and posterior (p) regions. Identification of anterior and posterior AOB regions can be done based on morphology and immunohistochemical markers. A–A′) Immunostainings against Nrp2 (green) and Robo2 (red) highlight the aAOB and pAOB, respectively. B–B′) Glomeruli throughout the AOB have varied composition of the cell surface molecules Kirrel2 (green) and Kirrel3 (red). C) Automated identification of glomeruli in anterior (C) and posterior (C′) regions based on VGluT2 (blue) immunostaining. D–D‴) High-magnification comparisons of automated selections after thresholding and manual selections of the same regions in anterior (D–D′) and posterior (D″–D‴) Dashed rectangle regions (B′, C, C′) indicate regions used for magnified comparisons for automated and manually selected glomeruli. E–G) Comparison of the normalized values from manual and automated glomeruli selections showed no statistically significant differences for the (E) average size of glomeruli, (F) number of glomeruli/section, and (G) immunoreactivity of Kirrel2 and Kirrel3 in anterior and posterior regions of an adult wild-type AOB.
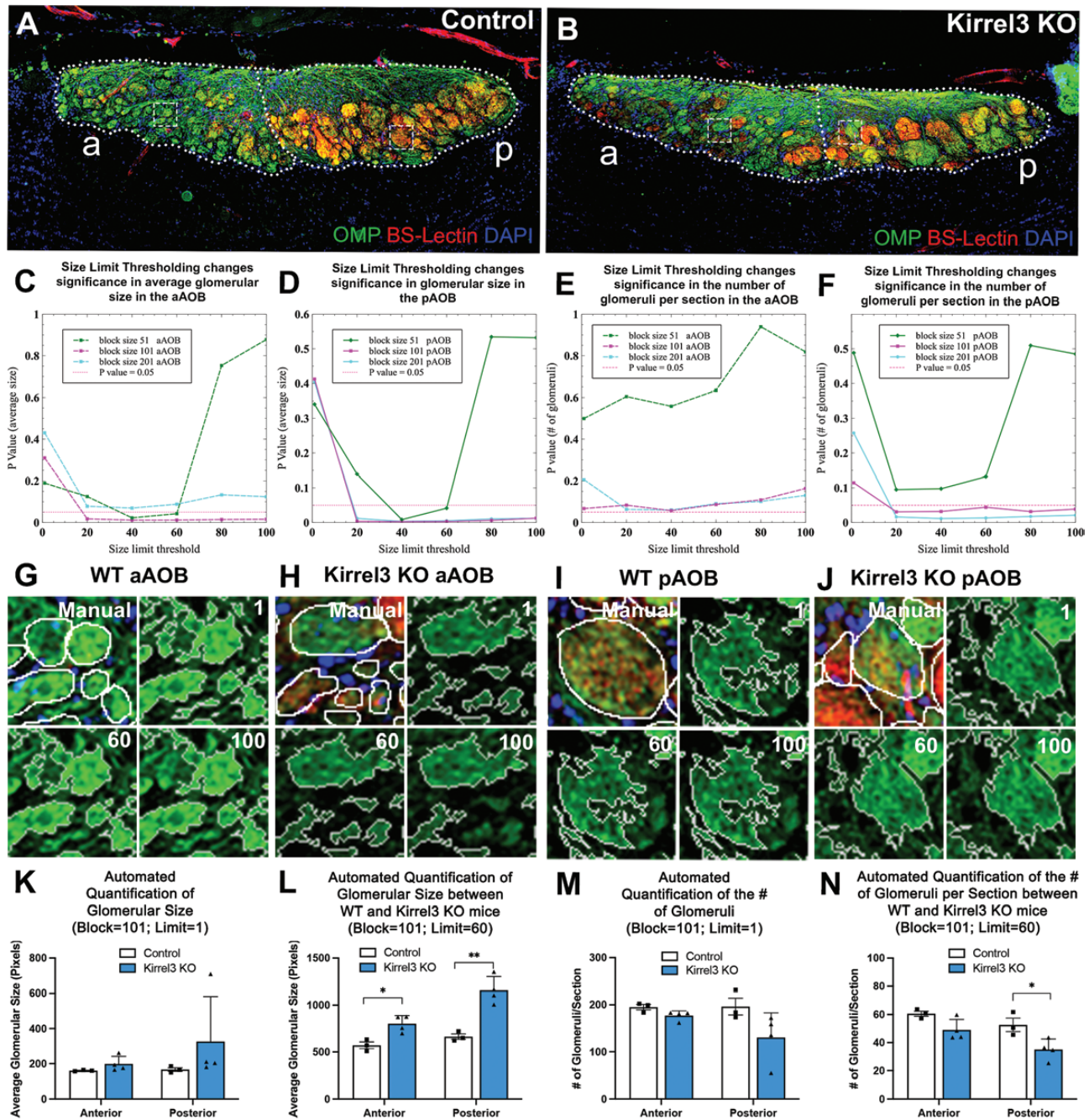
Fig. 4. Automated selection and analysis of glomeruli in Kirrel3 mutants and WT controls. A, B) The olfactory marker protein (OMP, green) immunostaining and the BS-Lectin (red) staining with a Hoescht (blue) counterstain on the AOBs of adult WT control (A) and Kirrel3 KO mutant (B). OMP is present throughout the fibers of all VSNs, while BS-lectin is more highly expressed by fibers in the posterior AOB. Dashed boxes indicate the regions magnified for comparison in (G–J). C–F) Resulting *P*-values when comparing WT and Kirrel3 KOs when using various settings for block size (51, 101, 201 pixels) and minimum size limit (1, 20, 40, 60, 80, 100 pixels). The resulting *P*-values for average glomeruli size in the aAOB (C) and pAOB (D), and for the average number of glomeruli per section in the aAOB (E) and pAOB (F). Horizontal red dotted line indicates *P*-value = 0.05. G–J) Comparison of manual tracing of the WT (I, K) and Kirrel3 KO (J, L) glomeruli in the anterior (G, H) and posterior (I, J) AOB to the automated identification of glomeruli at block size 101 pixels with minimum size limits at 1, 60, and 100 pixels. K–N) Automated quantification with block size 101 pixels for glomerular size (K, L) and number of glomeruli (M, N) without a minimum size limit (Limit = 1 pixel) (K, M). Small regions were included in the quantification, making any phenotypic differences across genotypes undetectable in both the anterior and posterior AOB. The same automated identification of glomeruli including a minimum size limit of 60 pixels (L, N) could detect differences in glomerular size (L) and number (N) in the WT and Kirrel3 mutant mice in the pAOB, as expected. Additionally, using these parameters, our program also detected significant differences in glomerular size in the anterior AOB, but no significant difference in the number of glomeruli.

applying consistent parameters across an entire image set. In order to optimize glomeruli detection starting from digital images that vary in quality and signal-to-noise ratio, we identified block size and minimum size limits as key parameters.

Optimization experiments for setting block size and minimum size limits should be performed for individual staining and sets of images as these could differ between labs for quality, contrast, resolution, and noise. As in manual quantification, avoiding saturation

of the images is fundamental and necessary for identification and selection of distinct regions by this program. Although the human eye may be able to infer the distinction between objects, even in a slightly saturated image, the program cannot make such distinctions, as it uses adaptive thresholding to identify regions with similar intensity in a single channel (data not shown).

Our program identifies putative glomeruli using consistent parameters, where an ROI define either an entire glomerulus or a portion of it according to the adaptive thresholding (Figs. 3D–D‴ and 4G–J). Notably, even though the shapes identified by manual and automated quantification appeared different, the normalized results from each method yielded comparable statistical significance (Fig. 3E–G). These data indicate that our system is sensitive enough to detect differences across genotypes and that using consistent parameters could facilitate the identification of subtle differences that can be lost due to the time constraints and variability between investigators.

Ethical statement

All mouse studies were approved by the University at Albany Institutional Animal Care and Use Committee (IACUC).

Conflict of interest

The authors declare that the research was conducted in the absence of any commercial or financial relationships that could be construed as a potential conflict of interest.

Funding

References

Beck DM, Kastner S. 2009. Top-down and bottom-up mechanisms in biasing competition in the human brain. *Vision Res*. 49(10):1154–1165.

Belluscio L, Koentges G, Axel R, Dulac C. 1999. A map of pheromone receptor activation in the mammalian brain. *Cell*. 97(2):209–220.

Bradski G. 2000. The OpenCV Library. *Dr Dobbs J Soft Tool*. 120:122–125.

Brignall AC, Cloutier JF. 2015. Neural map formation and sensory coding in the vomeronasal system. *Cell Mol Life Sci*. 72(24):4697–4709.

Bufe B, Schumann T, Zufall F. 2012. Formyl peptide receptors from immune and vomeronasal system exhibit distinct agonist properties. *J Biol Chem*. 287(40):33644–33655.

Chamero P, Katsoulidou V, Hendrix P, Bufe B, Roberts R, Matsunami H, Abramowitz J, Birnbaumer L, Zufall F, Leinders-Zufall T. 2011. G protein G(alpha)o is essential for vomeronasal function and aggressive behavior in mice. *Proc Natl Acad Sci USA*. 108(31):12898–12903.

Chamero P, Weiss J, Alonso MT, Rodríguez-Prados M, Hisatsune C, Mikoshiba K, Leinders-Zufall T, Zufall F. 2017. Type 3 inositol 1,4,5-trisphosphate receptor is dispensable for sensory activation of the mammalian vomeronasal organ. *Sci Rep*. 7(1):10260.

Cloutier JF, Giger RJ, Koentges G, Dulac C, Kolodkin AL, Ginty DD. 2002. Neuropilin-2 mediates axonal fasciculation, zonal segregation, but not axonal convergence, of primary accessory olfactory neurons. *Neuron*. 33(6):877–892.

Cosentino A, Boni E, Pacini S, Branca J, Morucci G, Ruggiero M, Bocchi L. 2015. Morphological analysis of neurons: automatic identification of elongations. *Annu Int Conf IEEE Eng Med Biol Soc*. 2015:8131–8134.

Dean C, Scholl FG, Choih J, DeMaria S, Berger J, Isacoff E, Scheiffele P. 2003. Neurexin mediates the assembly of presynaptic terminals. *Nat Neurosci*. 6(7):708–716.

Del Punta K, Leinders-Zufall T, Rodriguez I, Jukam D, Wysocki CJ, Ogawa S, Zufall F, Mombaerts P. 2002. Deficient pheromone responses in mice lacking a cluster of vomeronasal receptor genes. *Nature*. 419(6902):70–74.

Dominguez C, Heras J, Pascual V. 2017. IJ-OpenCV: combining ImageJ and OpenCV for processing images in biomedicine. *Comput Biol Med*. 84:189–194.

Dulac C, Axel R. 1995. A novel family of genes encoding putative pheromone receptors in mammals. *Cell*. 83(2):195–206.

Enomoto T, Ohmoto M, Iwata T, Uno A, Saitou M, Yamaguchi T, Kominami R, Matsumoto I, Hirota J. 2011. Bcl11b/Ctip2 controls the differentiation of vomeronasal sensory neurons in mice. *J Neurosci*. 31(28):10159–10173.

Lamprecht MR, Sabatini DM, Carpenter AE. 2007. CellProfiler: free, versatile software for automated biological image analysis. *Biotechniques*. 42(1):71–75.

Liberles SD, Horowitz LF, Kuang D, Contos JJ, Wilson KL, Siltberg-Liberles J, Liberles DA, Buck LB. 2009. Formyl peptide receptors are candidate chemosensory receptors in the vomeronasal organ. *Proc Natl Acad Sci USA*. 106(24):9842–9847.

Lin JM, Taroc EZM, Frias JA, Prasad A, Catizone AN, Sammons MA, Forni PE. 2018. The transcription factor Tfap2e/AP-2ε plays a pivotal role in maintaining the identity of basal vomeronasal sensory neurons. *Dev Biol*. 441(1):67–82.

Lutnick B, Ginley B, Govind D, McGarry SD, LaViolette PS, Yacoub R, Jain S, Tomaszewski JE, Jen KY, Sarder P. 2019. An integrated iterative annotation technique for easing neural network training in medical image analysis. *Nat Mach Intell*. 1(2):112–119.

Martin EA, Muralidhar S, Wang Z, Cervantes DC, Basu R, Taylor MR, Hunter J, Cutforth T, Wilke SA, Ghosh A, et al. 2015. The intellectual disability gene Kirrel3 regulates target-specific mossy fiber synapse development in the hippocampus. *Elife*. 4:e09395.

Meisami E, Bhatnagar KP. 1998. Structure and diversity in mammalian accessory olfactory bulb. *Microsc Res Tech*. 43(6):476–499.

Naik AS, Lin JM, Taroc EZM, Katreddi RR, Frias JA, Lemus AA, Sammons MA, Forni PE. 2020. Smad4-dependent morphogenic signals control the maturation and axonal targeting of basal vomeronasal sensory neurons to the accessory olfactory bulb. *Development*. 147:dev184036.

Obando DFG, Olivo-Marin J, Meas-Yedid V. 2018. Morphological operations on polygons using straight skeletons for digital pathology. In: 2018 IEEE 15th International Symposium on Biomedical Imaging (ISBI 2018). p. 1369–1372. doi:10.1109/ISBI.2018.8363826.

Otsu N. 1979. A threshold selection method from gray-level histograms. *IEEE Trans Syst Man Cybern*. 9:62–66.

Prince JE, Brignall AC, Cutforth T, Shen K, Cloutier JF. 2013. Kirrel3 is required for the coalescence of vomeronasal sensory neuron axons into glomeruli and for male-male aggression. *Development*. 140(11):2398–2408.

Prince JE, Cho JH, Dumontier E, Andrews W, Cutforth T, Tessier-Lavigne M, Parnavelas J, Cloutier JF. 2009. Robo-2 controls the segregation of a portion of basal vomeronasal sensory neuron axons to the posterior region of the accessory olfactory bulb. *J Neurosci*. 29(45):14211–14222.

Riviere S, Challet L, Fluegge D, Spehr M, Rodriguez I. 2009. Formyl peptide receptor-like proteins are a novel family of vomeronasal chemosensors. *Nature*. 459(7246):574–577.

Rizzardi AE, Zhang X, Vogel RI, Kolb S, Geybels MS, Leung YK, Henriksen JC, Ho SM, Kwak J, Stanford JL, et al. 2016. Quantitative comparison and reproducibility of pathologist scoring and digital image analysis of estrogen receptor β2 immunohistochemistry in prostate cancer. *Diagn Pathol*. 11(1):63.

Rodriguez I, Feinstein P, Mombaerts P. 1999. Variable patterns of axonal projections of sensory neurons in the mouse vomeronasal system. *Cell*. 97(2):199–208.

Serizawa S, Miyamichi K, Takeuchi H, Yamagishi Y, Suzuki M, Sakano H. 2006. A neuronal identity code for the odorant receptor-specific and activity-dependent axon sorting. *Cell*. 127(5):1057–1069.

Silvotti L, Cavalca E, Gatti R, Percudani R, Tirindelli R. 2011. A recent class of chemosensory neurons developed in mouse and rat. *PLoS One*. 6(9):e24462.

Stowers L, Holy TE, Meister M, Dulac C, Koentges G. 2002. Loss of sex discrimination and male-male aggression in mice deficient for TRP2. *Science*. 295(5559):1493–1500.

Uchida S. 2013. Image processing and recognition for biological images. *Dev Growth Differ*. 55(4):523–549.

Vaddadi N, Iversen K, Raja R, Phen A, Brignall A, Dumontier E, Cloutier JF. 2019. Kirrel2 is differentially required in populations of olfactory sensory neurons for the targeting of axons in the olfactory bulb. Development. 146(11):dev173310. doi:10.1242/dev.173310

Zapiec B, Mombaerts P. 2015. Multiplex assessment of the positions of odorant receptor-specific glomeruli in the mouse olfactory bulb by serial two-photon tomography. *Proc Natl Acad Sci USA*. 112(43):E5873–E5882.